

A composite solution to the EDGES anomaly

Anubhav Mathur,¹ Surjeet Rajendran,¹ and Harikrishnan Ramani²

¹*Department of Physics and Astronomy, Johns Hopkins University,
3400 N. Charles St., Baltimore, MD 21218, USA*

²*Stanford Institute for Theoretical Physics, Stanford University, Stanford, CA 94305, USA*

Subcomponent millicharged dark matter that cools baryons via Coulomb interactions has been invoked to explain the EDGES anomaly. However, this model is in severe tension with constraints from cosmology and stellar emissions. In this work, we consider the consequences of these millicharged particles existing in composite blobs. The relevant degrees of freedom at high temperature are minuscule elementary charges, which fuse at low temperatures to make up blobs of larger charge. These blobs serve as the degrees of freedom relevant in cooling the baryons sufficiently to account for the EDGES anomaly. In such a model, cosmology and stellar constraints (which involve high-temperature processes) apply only to the feebly-interacting elementary charges and not to the blobs. This salvages a large range of parameter space for millicharged blobs that can explain the EDGES anomaly. It also opens up new parameter space for direct detection, albeit at low momentum transfers.

I. INTRODUCTION

The Experiment to Detect the Global Epoch of Reionization Signature (EDGES) experiment has reported a dip in the 21 cm spectrum corresponding to strong absorption around $z = 17$ [1]. This can be interpreted as a 3.8σ deviation from the Λ CDM prediction for the baryon temperature [2–4]. Dark matter (DM) cooling of the baryonic fluid has been invoked as an explanation for this excess [2–4]. A DM model that maximizes the cross-section around cosmic dawn is sub-component millicharged dark matter (mCDM), which has a larger cross-section with Standard Model (SM) charges at the lowest relative velocities. However, the millicharge parameter space is extremely constrained due to limits from CMB and BBN, cooling of SN1987A and stars, and terrestrial experiments [4]. It has subsequently been shown that even this limited parameter space results in overproduction of mCDM through freeze-in [5, 6].

These difficulties have led to two other ways to solve the EDGES anomaly. The first involves heating the CMB relative to baryons [7–10], while the second involves mCDM which is tightly coupled to an additional cold component that forms the dominant DM which does the bulk of the cooling [11]. In this paper, we point to a third possibility. The mCDM explanations for the EDGES anomaly to date have treated the millicharged particle (mCP) as elementary without internal structure. As a result, the same mCP is the physical particle at all energies. In this work, we explore the consequence of this mCP being a composite state of elementary mCPs with much smaller mass and charge, glued together by a force that confines at low temperatures. The elementary charges are the relevant degrees of freedom at temperatures and energies much higher than cosmic dawn. As a result, in our model, constraints from CMB, BBN, overclosure, stellar and SN cooling as well as colliders all apply only to the elementary charges. We demonstrate here that there is a drastic increase in new parameter space for mCDM as long as it is in a composite state

(blob). Furthermore, we explore the quirky thermal history for the dark sector that involves confinement when T_D (the dark temperature) falls below Λ_D (the dark confining scale) and deconfinement if the dark temperature increases subsequently. We point out a novel dark phase where thermal contact with the SM results in a thermostatic dark bath, i.e. the dark bath staying at the same temperature with the heat dump from baryons exactly cancelled by Hubble cooling.

II. MODEL

We consider elementary mCP fermions that carry electric charge ϵ_f and mass m_f with a confining force that confines at $\Lambda_D \lesssim m_f$. We also assume that the mCPs are charged under a dark $U(1)$ with a dark charge g_D . This dark $U(1)$ accomplishes two goals: first, it allows the electric charge of the mCP to be generated via kinetic mixing and second, it provides Coulomb repulsion that prevents blobs from getting too big. The mass of the dark photon is unimportant as long as it is sufficiently long ranged to allow the blobs to interact with baryons via Coulomb scattering. We can take this mass to be zero, or low enough to evade direct stellar constraints on the dark photon.

For simplicity we will assume that these elementary mCPs that confine all have the same charge sign. For net neutrality, we envision an asymmetric dark “leptonic” component with the opposite charge that is not charged under this confining gauge group, just like the leptons in the SM which are singlets under strong interactions. We further assume that the elementary charges confine to form composite blobs with “atomic number” A such that the composites χ carry charge $\epsilon_\chi = A\epsilon_f$. The mass of these blobs are roughly $m_\chi = A(m_f - \Lambda_D)$ i.e. the difference between the total mass of the constituents minus the binding energy. Since $m_f \gtrsim \Lambda_D$, we approximate this to $m_\chi = Am_f$. These mCP blobs also have non-zero

size [12]

$$R_{\text{blob}} = \frac{A^{\frac{1}{3}}}{\Lambda_D} \quad (1)$$

We describe the highlights of the phenomenology of this setup in sub-section II A. These aspects of the phenomenology are quantitatively shown in sections II B and II C.

A. Synopsis of Blob Evolution

We start by assuming that the temperature T_D of the blobs is lower than the confining scale Λ_D . Assuming we are in the early universe where the baryon temperature $T_b \gg \Lambda_D$. We take the elementary mCPs to have a low enough charge that they are not in thermal equilibrium in the early universe. The cold elementary mCPs will begin to fuse and form larger blobs. As the blobs become bigger, they will interact with the baryons and start extracting energy from the standard model leading to heating of the blob sector. But, the temperature of this sector cannot get larger than Λ_D since the blobs are not confined above this temperature. This implies that only a small fraction of the mCPs are actually able to fuse and become blobs in the early universe. Further, the maximum size of the blobs during this phase is set by Coulomb repulsion—as the blob becomes larger, the repulsion from the dark $U(1)$ grows and it inhibits the ability of elementary mCPs to fuse with the blob.

This scenario continues until T_b drops sufficiently so that it is unable to transfer enough heat to inhibit blob growth. At this stage, there is rapid fusion of the mCPs creating blobs, resulting in most of the mCPs ending up in blobs. The maximum size of the blob in this case is also set by Coulomb repulsion.

Parameters are chosen so that this phase of blob formation occurs around the redshifts of interest to the EDGES experiment. At this stage, the blobs scatter with the baryons, cooling the baryons and explaining the EDGES observations.

B. The Size of the Blob

It is necessary to limit the size of the blobs so that they can coherently scatter with the baryons, maximizing the heat transfer between the two fluids. The dark $U(1)$ provides the Coulomb repulsion necessary to enforce this limit. Since $g_D \gg \epsilon_f$, we will ignore the Coulomb repulsion from electromagnetism in this section.

How do the blobs form? We follow the prescription developed in [13], but modify it to account for the Coulomb repulsion due to the dark $U(1)$ [14]. Initially, individual partons merge to form states with atomic number 2. We call this the $\{1, 1\}$ stage. This process can be inefficient since it requires the emission of some other degree of

freedom to make up for the reduced phase space for the $2 \rightarrow 1$ process. For the parameter space we consider, this is still more rapid than Hubble expansion. But, once objects with atomic number 2 are formed, the blobs can grow quickly¹ Unlike the case considered in [13], in our case as the blobs grow bigger, there is an increased Coulomb barrier to fusion as treated in [14]. Consider two cases: the fusion of two large blobs, which we refer to as $\{A, A\}$, or a large blob and a small blob which we refer to as $\{A, 1\}$. The cross-section for fusion is proportional to the geometric surface area of the blob. But, as the blobs become larger, this cross-section is suppressed by the Coulomb barrier. Parametrically, this cross-section can be expressed as:

$$\sigma_{A,A'} = \sigma_0 (\text{Max}(A, A'))^{\frac{2}{3}} P_G(T) \quad (2)$$

where σ_0 is the base fusion cross-section $\sim \Lambda_D^{-2}$ and $P_G(T)$ is the Gamow factor [15] which is the temperature dependent factor that captures the effects of the Coulomb barrier. This factor is:

$$P_G(T) = e^{-G_E} = e^{-\sqrt{\frac{2\mu Q_1^2 Q_2^2}{T_D}}} \quad (3)$$

Here Q_1 and Q_2 are the charges $A_{1,2} \times g_D$ of the two blobs respectively and μ is their reduced mass. Thus fusion freeze-out depends critically on the Gamow factor. From the Gamow factor, it is clear that $\{A, 1\}$ fusion will dominate over $\{A, A\}$ type fusion due to weaker Coulomb repulsion. Moreover, as the blobs grow in size, the number density of larger blobs is lower than that of smaller blobs. Further the cross-section for a smaller blob to merge with a larger blob is set by the geometric size of the larger blob. All of these factors imply that the growth of the blobs in our case is dominated by the mergers of small blobs with larger blobs *i.e.* processes of type $\{A, 1\}$.

Let us now see how big these blobs can get *i.e.* estimate the freeze out of the fusion process. It can easily be verified that for the parameters of interest to this paper, in the absence of the exponentially suppressed Gamow factor, the rate of the fusion process is very rapid compared to Hubble. The size of the blob is then restricted purely by the exponential suppression from the Gamow factor which forces the process to freeze out.

Taking $T_D \approx \mu \approx \Lambda_D$, for $\{A, 1\}$ fusion, the Gamow exponent is

$$G_E \approx A g_D^2 \quad (4)$$

This places a bound on fusion growth,

$$A_{\text{Gamow}}^{\text{lim}} \approx g_D^{-2} \quad (5)$$

¹ The ratio of fusion rate to Hubble rate for $\{A, A\}$ fusion is

$$\frac{n\sigma v}{H} = \frac{10^{32} f_D z^{\frac{3}{2}}}{A^{\frac{3}{2}}} \left(\frac{10 \text{ K}}{\Lambda_D} \right)^2 \sqrt{\frac{T_D}{10 \text{ K}}} \left(\frac{10 \text{ K}}{m_f} \right)^3 \gg 1$$

This limit on the blob size arising from the inhibition of their growth is stronger than the stability limit [12] $A_{\text{stab}}^{\text{lim}} = 1/g_D^3$ that can be placed on their size due to Coulomb repulsion. Blob freeze out occurs only due to the exponential dependence on blob size in the Gamow factor. Thus, blobs whose sizes are close to, but smaller than the Gamow limit are rapidly formed. This implies that as the universe expands and the temperatures drop, blobs will continue to grow until the Gamow limit is reached.

It is also important to consider the heat that is released by the fusion process as the blobs grow. Each fusion process that occurs in $\{A, 1\}$ fusion releases energy $\sim \Lambda_D$. Thus in the roughly $\sim A$ fusion processes that occur to form a blob of size A , approximately $A\Lambda_D$ energy into $\sim A$ particles is released. Thus the heat released in the fusion cannot change the temperature by more than Λ_D and thus does not hinder fusion.

While we expect this mechanism to produce a range of blob masses, the charge to mass ratio of all these blobs is the same. As seen later in Sec. IV, for most of the relevant parameter space, results depend only on the charge to mass ratio, so it is justified to make a simplifying assumption that all blobs are of the same mass m_χ . Note that this analysis of the blob size is independent of the baryon temperature T_b . As we show in the following section, T_b is an important parameter in determining the number of mCPs that are fused into blobs but it does not determine the maximum size of a blob.

C. Heat Transfer

In order to understand heat transfer with the SM bath, we start by deriving the transfer cross-section for blobs and elementary charges to scatter with baryons.

The differential cross-section for a mCP with charge e to scatter with protons/electrons is [16],

$$\frac{d\sigma}{d\cos\theta} = \frac{2\pi e^2 \alpha^2}{\mu^2 v_{\text{rel}}^4 (1 - \cos\theta)^2}. \quad (6)$$

with μ the reduced mass and v_{rel} the relative velocity.

The forward divergence is cut off by the Debye mass of the mediator. For the SM photon, the Debye mass squared is given by

$$\Pi_A = e^2 \left(\frac{x_e n_b}{T_b} \right) \quad (7)$$

where $x_e \equiv n_e/n_H$ is the free-electron fraction, determined using [17, 18]. The Debye mass is approximately 10^{-6} eV at $z = 1000$ and 3×10^{-8} eV at $z = 10$. The Debye mass square of the dark photon is

$$\Pi_{A'} = g_D^2 \left(\frac{n_D}{T_D} \right) \quad (8)$$

For the parameter space we are interested in, $g_D^2 n_D \ll e^2 x_e n_b$ and $T_D \leq T_b$, such that $\Pi_{A'} \ll \Pi_A$. Hence we

take only the SM photon Debye mass to regulate the divergence.

Finally, for elementary charges, $q_{\text{max}} = 2\mu v_{\text{rel}}$, such that the θ integral is taken between the limits $\theta = \{-1, \frac{2e\alpha\sqrt{\Pi_A}}{3T_b}\}$. For blobs, $q_{\text{max}} \sim \text{Min}(R_{\text{blob}}^{-1}, 2\mu v_{\text{rel}})$, such that $\theta_{\text{min}} = 1 - \frac{q_{\text{max}}^2}{2\mu^2 v_{\text{rel}}^2}$. The thermal-averaged transfer cross-section in the $q_{\text{max}}^2 \gg \Pi_A$ limit is given by integrating Eqn. 6 over θ , giving,

$$\sigma_T = \frac{2\pi e^2 \alpha^2 \xi}{\mu^2 v_{\text{rel}}^4} \quad (9)$$

with $\xi = \ln\left(\frac{9T_b^3}{4\pi e^2 \alpha^3 x_e n_b} \frac{q_{\text{max}}^2}{2\mu^2 v_{\text{rel}}^2}\right)$. In the region of interest, it is safe to ignore the factor $\frac{q_{\text{max}}^2}{2\mu^2 v_{\text{rel}}^2}$ since it is inside the log.

Next, we compare the rate of charges scattering off baryons to the Hubble rate,

$$\frac{n_b \sigma_T v_{\text{rel}}}{H} \approx 10^{-18} \left(\frac{\epsilon_f}{10^{-14}} \right)^2 z^{\frac{3}{2}} \left(\frac{10 \text{ K}}{T_D} \right)^2 \quad (10)$$

As a result, the elementary charges ϵ_f which we take to obey stellar-cooling constraints discussed next in Eqn. 15, are never in thermal contact with the SM. We also see that blobs with charge $\epsilon_\chi \gtrsim 10^{-7}$ can interact with the SM bath.

At temperatures around $T_D \approx \Lambda_D$, both elementary charges and blobs can co-exist. Defining $\mathcal{F}_{\text{blob}}(z)$ as the fraction of millicharges that are in the blob phase, we get

$$\begin{aligned} \dot{T}_D^{\text{ref}}(\mathcal{F}_{\text{blob}}) = & -2HT_D + \frac{2}{3} \frac{m_\chi x_e \rho_b}{(m_\chi + m_b)^2} \mathcal{F}_{\text{blob}} \frac{\sigma_0}{u_{\chi,b}^3} \\ & \times \left\{ \sqrt{\frac{2}{\pi}} (T_b - T_D) \right\} \end{aligned} \quad (11)$$

Here $u_{\chi,b} = \sqrt{\frac{T_D}{m_\chi} + \frac{T_b}{m_b}}$ is the average relative velocity due to thermal motion and $\sigma_0 = \sigma_T v_{\text{rel}}^4$. We have verified that the bulk relative velocity between the χ bath and SM fluids does not contribute substantially to the thermal evolution of either fluid.

When $T_D \gtrsim \Lambda_D$, the relevant degrees of freedom are the elementary charges, which have no thermal contact with the SM such that the dark fluid cools due to Hubble expansion. When T_D drops below Λ_D there is rapid blob formation. These blobs can now interact with the SM and heat up, but the temperature cannot exceed T_D ; after all, thermal contact with the SM would immediately be lost. Consequently if the second term in Eqn. 11 dominates for $\mathcal{F}_{\text{blob}} \rightarrow 1$, then $\mathcal{F}_{\text{blob}}$ adjusts to smaller values so as to keep $\dot{T}_D = 0$. Thus, we set

$$\dot{T}_D = \begin{cases} \text{Min}\left(0, \dot{T}_D^{\text{ref}}(\mathcal{F}_{\text{blob}} = 1)\right) & T_D \geq \Lambda_D \\ \dot{T}_D^{\text{ref}}(\mathcal{F}_{\text{blob}} = 1) & T_D < \Lambda_D \end{cases}$$

In the regime where $\dot{T}_D = 0$, we can solve for the z dependent fraction in blobs $\mathcal{F}_{\text{blob}}$ by setting Eqn. 11 to 0. We find for $T_D \geq \Lambda_D$,

$$\mathcal{F}_{\text{blob}} = \text{Min} \left(1, 2HT_D \times \left[\frac{2}{3} \frac{m_\chi x_e \rho_b}{(m_\chi + m_b)^2} \frac{\sigma_0}{u_{\chi,b}^3} \times \left\{ \sqrt{\frac{2}{\pi}} (T_b - T_D) \right\} \right]^{-1} \right) \quad (12)$$

We can see that in the limit where $T_b \gg T_D$, and when interactions are strong enough, the quantity in square brackets is much larger than Hubble cooling and hence $\mathcal{F}_{\text{blob}} \rightarrow 0$. This happens because in this limit, blobs that form immediately break up into elementary charges. As the disparity between T_b and T_D shrinks, $\mathcal{F}_{\text{blob}} \rightarrow 1$.

The time evolution of the baryon temperature obeys

$$\dot{T}_b = -2HT_b + \frac{2}{3} \frac{m_b x_e \rho_D}{(m_\chi + m_b)^2} \frac{\mathcal{F}_{\text{blob}} f_D}{1 + f_{\text{He}} + x_e} \frac{\sigma_0}{u_{\chi,b}^3} \times \left\{ \sqrt{\frac{2}{\pi}} (T_D - T_b) \right\} + \Gamma_C (T_{\text{CMB}} - T_b) \quad (13)$$

where $f_{\text{He}} \equiv n_{\text{He}}/n_{\text{H}}$ is the helium fraction and Γ_C is the Compton scattering rate.

The initial conditions we use are

$$\begin{aligned} T_b(z = 1000) &= T_{\text{CMB}}(z = 1000) \approx T_{\text{CMB}}^0 \times 1000 \\ T_{\text{CMB}}^0 &= 2.725 \text{ K} \\ T_D(z = 1000) &= 0 \text{ K} \end{aligned} \quad (14)$$

Setting the initial dark temperature to 0 K is not physical, but is accurate because the time evolution rapidly adjusts the temperature to its correct value just below $z = 1000$.

III. EXISTING LIMITS

As alluded to in the introduction, the constraints on composite mCPs can be quite different from elementary mCPs of the same charge. We elucidate further below.

Stellar bounds: For $\Lambda_D \ll 1 \text{ keV}$, the relevant degrees of freedom in the interior of stars and supernovae are the elementary mCPs, and their charge is restricted to $\epsilon_f < 10^{-14}$ for small enough m_f . The blobs are never produced in stellar environments. However the limit on the elementary charges translates to a limit on blob charge:

$$\epsilon_\chi < 10^{-14} \frac{m_\chi}{\Lambda_D}. \quad (15)$$

BBN and CMB N_{eff} : As we have seen in the previous section, when there is significant thermal

contact with baryons and $T_b \gg \Lambda_D$, $\mathcal{F}_{\text{blob}} \rightarrow 0$ and the relevant degrees of freedom are the elementary charges before recombination. Thermal equilibrium with the SM is reached only if [6, 19] $\epsilon_f \gtrsim 10^{-8} \left(\frac{m_\chi}{10 \text{ K}} \right)^{\frac{1}{2}}$. This is more restrictive than stellar constraints only when $m_f \approx \Lambda_D \leq 1 \text{ } \mu\text{eV}$. Dark photons arising from bremsstrahlung and mesons from dark fusion are produced at the temperature of the dark bath and hence do not contribute appreciably to N_{eff} either.

CMB power spectrum: The effect of mCP scattering on protons was investigated in [4], and constraints from Planck 2015 data effectively ruled out mCPs as a solution to EDGES for $f_D > 0.4\%$. It is interesting to note that since these limits only depend on the charge to mass ratio $\frac{\epsilon_\chi}{m_\chi}$, they apply equally to blobs as well as elementary charges. However, it was found in [4] that no limits exist for $f_D \leq 0.4\%$, so we restrict ourselves to smaller fractions.

IV. RESULTS

We now display results obtained by numerically solving the coupled differential equations for time evolution. We consider a benchmark blob mass $m_\chi = 1 \text{ MeV}$, and charge $\epsilon_\chi = 4 \times 10^{-6}$ and $f_D = 0.4\%$. We start by tracking $\mathcal{F}_{\text{blob}}(z)$ for different Λ_D in Fig. 1. For large z , heat from the baryonic bath disintegrates the blobs rendering $\mathcal{F}_{\text{blob}} \ll 1$. For lower z , cooling due to Hubble expansion begins to dominate, resulting in larger values of $\mathcal{F}_{\text{blob}}$. For the same z , we see that as Λ_D is reduced, a smaller fraction of the dark bath exists in blobs as it is easier to break them apart.

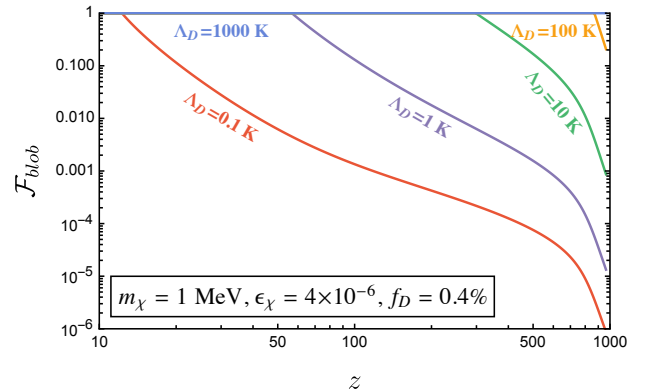


FIG. 1. The evolution of the fraction of the dark millicharged bath in blobs as a function of redshift is shown for different Λ_D , the dark confining scale. Smaller Λ_D leads to smaller blob fractions.

In Fig. 2, the time evolution of the baryonic temperature T_b and the dark temperature T_D are shown for different choices of Λ_D , the dark confining scale. The CMB temperature T_{CMB} and the baryon temperature T_b

in the absence of interacting DM are shown in black for reference. The colored solid lines correspond to different choices of Λ_D . We see that models with smaller Λ_D stay at the same temperature $T_D = \Lambda_D$ for longer. If these charges were elementary, the dark temperature would be higher than Λ_D in this regime. Instead, for blobs, this is prevented by the rapid break up of blobs with the resulting elementary charges losing thermal contact with the SM, cooling rapidly, and forming blobs again. The dashed solid lines track the baryonic temperature for different Λ_D . The baryonic temperature at $z = 17$ is roughly constant for different Λ_D . However, there is a small enough $\Lambda_D \approx 0.1\text{K}$, below which $\mathcal{F}_{\text{blob}}$ is too small even at $z = 17$, as seen in Fig. 1 and results in lower cooling of T_b in Fig. 2.

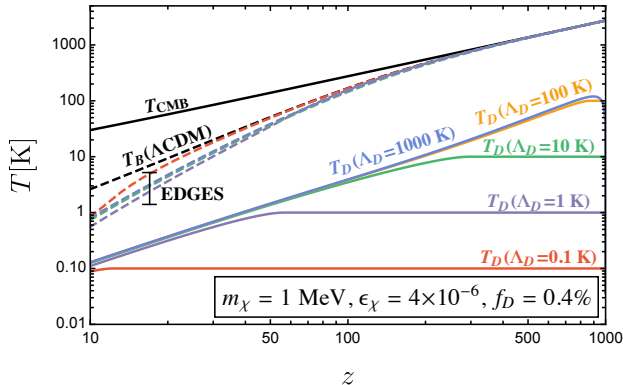


FIG. 2. Temperature evolution of the baryonic and DM bath are plotted as a function of redshift z . The CMB temperature and the baryon temperature without DM are plotted in black. The solid lines track the evolution of the dark temperature T_D for different Λ_D , the dark confining temperature. The dashed lines track the baryon temperature T_b for different Λ_D with the same color code as T_D . The error bar marks the baryonic temperature at $z = 17$ as measured by the EDGES collaboration.

We next discuss the contours that explain EDGES in the ϵ_χ vs m_χ plane and compare it to the parameter space derived for elementary charges in [19]. Given a DM fraction, elementary charges that explain EDGES obey $\epsilon_{\text{elem}} \propto m_{\text{elem}}$ as seen with the black curve. This happens due to the following reason. For a fixed DM fraction, a drop in T_b , ΔT_b is associated with an increase in dark temperature $\Delta T_D \propto m_{\text{elem}} \times \Delta T_b$, i.e. larger elementary masses m_{elem} undergo larger temperature gain because of equipartition. Another way to see this is that the total energy gained is equal to $n_{\text{elem}} \times \Delta T_D$ and the number density is inversely proportional to m_{elem} , and hence T_D is directly proportional to m_{elem} . Starting with an initially-cold dark bath $T_D \ll T_b$, the proportionality factor ensures that $T_D \propto m_{\text{elem}}$ throughout. This in turn implies that the elementary charges' thermal velocity is independent of the mCP mass. Finally, the heat transfer is proportional to the transfer cross-section given in Eqn. 9, which is dependent only on the charge to mass

ratio since the velocity is mass-independent. Thus, this behavior applies to very small masses. It was also pointed out in [19] that for a choice of DM fraction, there is also a maximum mass due to the same equipartition arguments, $m_{\text{elem}} \leq \mu_b f_{\text{elem}} \Omega_c / \Omega_b$. The elementary charge required to explain EDGES obeys [19],

$$\epsilon_{\text{elem}} \approx 6 \times 10^{-7} \frac{m_{\text{elem}}}{\text{MeV}} \left(\frac{10^{-2}}{f_{\text{elem}}} \right)^{\frac{3}{4}}. \quad (16)$$

It is important to note that the entirety of the elementary charge solution is ruled out [6].

Next we discuss the contours for blobs for different Λ_D . In each case, we mark out the unphysical region where the elementary charges required to create blobs are ruled out by stellar constraints from Eqn. 15. For the same reason as explained for the elementary charge solution, we observe a linear relationship $\epsilon_\chi \propto m_\chi$ for the blobs as well. This linear regime obeys an approximate empirical relation

$$\epsilon_\chi \approx 10^{-6} \frac{m_\chi}{\text{MeV}} \left(\frac{10^{-2}}{f_\chi} \right)^{1.18}. \quad (17)$$

Once again, there exists a cut-off mass, that is now Λ_D dependent. For smaller Λ_D , the mCP bath stays elementary for longer, i.e. $\mathcal{F}_{\text{blob}} \ll 1$ for longer. To compensate, smaller blob mass m_χ is required to increase heat capacity, so as to reach temperatures below Λ_D sufficiently soon. As a corollary, larger Λ_D results in an enhanced range in mass where the EDGES solution is viable. However, larger Λ_D translates to stricter stellar constraints and for large enough Λ_D , the charge required to explain EDGES, Eqn. 17 is ruled out by Eqn. 15.

The blobs in most of the parameter space shown in Fig. 3 do not survive galaxy formation. The parameter space for which blobs do not break up in the galaxy is given in Eqn. 19 and can be recast as,

$$m_\chi^{\text{gal}} \lesssim 86 \text{ eV} \frac{\Lambda_D}{1 \text{ K}} \quad (18)$$

Thus even for $\Lambda_D \approx 10 \text{ K}$, the blobs resize themselves to masses below 1 keV, making prospects for direct detection tricky.

V. CONCLUSION

Making mCDM inherently composite is a simple nuance with parallels in SM baryons. In this work, we have considered this possibility and explored its myriad consequences with specific emphasis on explaining the EDGES anomaly.

The DM degrees of freedom are blobs at temperatures below the confining scale and elementary charges at temperatures above it. For an appropriately chosen confining scale Λ_D , the elementary charges are the degrees of

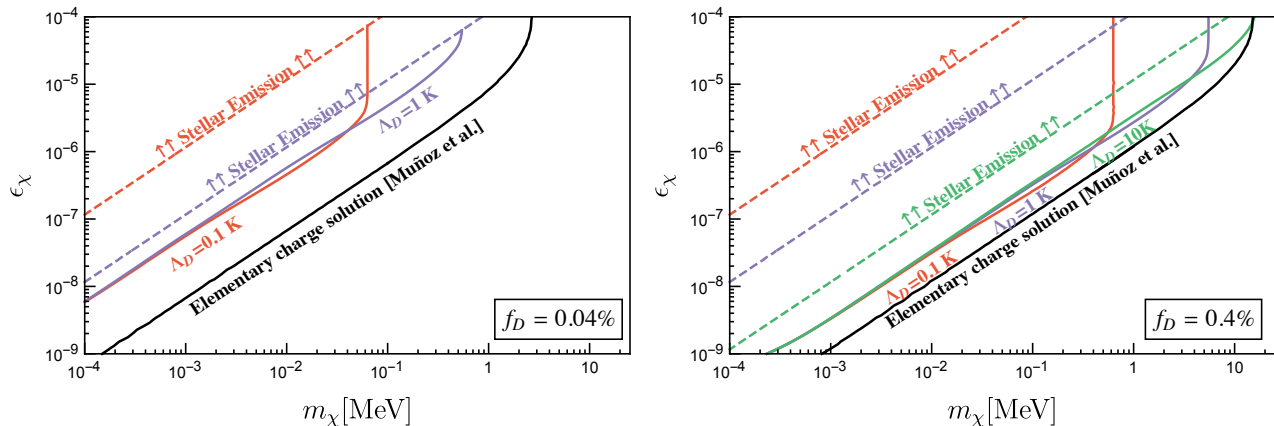


FIG. 3. The contours that explain the EDGES anomaly in the blob charge ϵ_χ vs blob mass m_χ plane are shown for different choices of the confining scale Λ_D for mCP bath fractions of $f_D = 0.04\%$ (left) and $f_D = 0.4\%$ (right). Also shown are stellar cooling constraints from Eqn. 15. The elementary charge solution from [19] is shown in black.

freedom during BBN, CMB and in the interior of stars. The elementary charges are chosen to be feeble enough to evade all these constraints. However, at temperatures below the confining scale, these rapidly fuse into blobs increasing in size till they reach a size determined by stability considerations due to repulsion. These blobs now have large enough charges that coherently scatter with baryons at temperatures around $z = 17$, relevant for physics during the dark ages, without suffering from the strict stellar and cosmology constraints that apply to elementary mCPs. Thus, we find a large unconstrained parameter space for mCP blobs for $f_D \leq 0.4\%$, that explains the EDGES anomaly. In the next few years, this signal will also be accessible to a slew of experiments sensitive to the global 21 cm signal such as SARAS2 [20], LEDA [21], SCI-HI/PRIZM [22], HYPERION [23] and CTP [24].

We also find that there is a novel dark phase, where the dark bath can exist as an admixture of elementary charges that do not interact with baryons and composite blobs that do, with the fraction in each adjusting so as to balance the heat transfer from baryons with cooling due to Hubble expansion. This keeps the dark bath at a constant temperature until the baryons become cool enough that Hubble cooling dominates heat transfer from baryons. While this phase was an intriguing curiosity in this work, in the early universe this can have interesting consequences to thermal freeze-out of mCPs with a confining force.

Finally, the avoidance of stellar and cosmology constraints due to the composite nature of the DM blobs provides a vastly larger parameter space that is unconstrained compared to elementary mCPs that do not confine. It is interesting to ask if these blobs can be probed in terrestrial experiments. This task is made more difficult by the fact that galaxy formation has the potential to destabilize the blobs. Galaxy formation results in DM gaining virial velocities $v_{\text{vir}} \approx 10^{-3}$. Self-

interactions are large enough to break up the blobs once more if the kinetic energy exceeds the confining scale. Thus the blobs stay intact till today only if

$$m_\chi v_{\text{vir}}^2 \lesssim \Lambda_D. \quad (19)$$

Hence, for large enough blob masses m_χ , there is significant fission in galaxies, the blobs are resized into smaller ones that obey Eqn. (19) which are present in the galaxy today. These smaller blobs should nevertheless be present in the galaxy today since the dark photon sets the range for self-interactions [25] and cuts off long-range galactic processes such as evacuation from the galactic disk [26, 27] and retention in galactic magnetic fields [28], and prevents the mCP from being blown away by the solar wind [27, 29].

This parameter space increases the scope of direct detection experiments sensitive to masses lower than 1 MeV, albeit at momentum transfers smaller than R_{blob}^{-1} to retain coherence. Experiments such as SENSEI [30], DAMIC [31], super-CDMS [32], and even future proposals [33–36] are not sensitive to momentum transfers $q \leq \Lambda_D \approx \text{meV}$. Instead, manipulation with electric and magnetic fields [37] is a promising detection strategy. For large enough blob charge, terrestrial accumulation and subsequent detection [38] might be a viable avenue.

ACKNOWLEDGMENTS

We thank Asher Berlin, Diego Redigolo, Gordan Krnjaic and Hongwan Liu for useful discussions. SR is supported in part by the NSF under grant PHY-1818899. SR is also supported by the DoE under a QuantISED grant for MAGIS and the SQMS quantum center. HR is supported in part by NSF Grant PHY-1720397 and the Gordon and Betty Moore Foundation Grant GBMF7946.

-
- [1] Judd D. Bowman, Alan E. E. Rogers, Raul A. Monsalve, Thomas J. Mozdzen, and Nivedita Mahesh, “An absorption profile centred at 78 megahertz in the sky-averaged spectrum,” *Nature* **555**, 67–70 (2018), arXiv:1810.05912 [astro-ph.CO].
- [2] Rennan Barkana, “Possible interaction between baryons and dark-matter particles revealed by the first stars,” *Nature* **555**, 71–74 (2018), arXiv:1803.06698 [astro-ph.CO].
- [3] Rennan Barkana, Nadav Joseph Outmezguine, Diego Redigolo, and Tomer Volansky, “Strong constraints on light dark matter interpretation of the EDGES signal,” *Phys. Rev. D* **98**, 103005 (2018), arXiv:1803.03091 [hep-ph].
- [4] Ely D. Kovetz, Vivian Poulin, Vera Gluscevic, Kimberly K. Boddy, Rennan Barkana, and Marc Kamionkowski, “Tighter limits on dark matter explanations of the anomalous EDGES 21 cm signal,” *Phys. Rev. D* **98**, 103529 (2018), arXiv:1807.11482 [astro-ph.CO].
- [5] Asher Berlin, Dan Hooper, Gordan Krnjaic, and Samuel D. McDermott, “Severely Constraining Dark Matter Interpretations of the 21-cm Anomaly,” *Phys. Rev. Lett.* **121**, 011102 (2018), arXiv:1803.02804 [hep-ph].
- [6] Cyril Creque-Sarbinowski, Lingyuan Ji, Ely D. Kovetz, and Marc Kamionkowski, “Direct millicharged dark matter cannot explain the EDGES signal,” *Phys. Rev. D* **100**, 023528 (2019), arXiv:1903.09154 [astro-ph.CO].
- [7] Chang Feng and Gilbert Holder, “Enhanced global signal of neutral hydrogen due to excess radiation at cosmic dawn,” *Astrophys. J. Lett.* **858**, L17 (2018), arXiv:1802.07432 [astro-ph.CO].
- [8] A. Ewall-Wice, T. C. Chang, J. Lazio, O. Dore, M. Seifert, and R. A. Monsalve, “Modeling the Radio Background from the First Black Holes at Cosmic Dawn: Implications for the 21 cm Absorption Amplitude,” *Astrophys. J.* **868**, 63 (2018), arXiv:1803.01815 [astro-ph.CO].
- [9] Maxim Pospelov, Josef Pradler, Joshua T. Ruderman, and Alfredo Urbano, “Room for New Physics in the Rayleigh-Jeans Tail of the Cosmic Microwave Background,” *Phys. Rev. Lett.* **121**, 031103 (2018), arXiv:1803.07048 [hep-ph].
- [10] Anastasia Fialkov and Rennan Barkana, “Signature of Excess Radio Background in the 21-cm Global Signal and Power Spectrum,” *Mon. Not. Roy. Astron. Soc.* **486**, 1763–1773 (2019), arXiv:1902.02438 [astro-ph.CO].
- [11] Hongwan Liu, Nadav Joseph Outmezguine, Diego Redigolo, and Tomer Volansky, “Reviving Millicharged Dark Matter for 21-cm Cosmology,” *Phys. Rev. D* **100**, 123011 (2019), arXiv:1908.06986 [hep-ph].
- [12] Dorota M. Grabowska, Tom Melia, and Surjeet Rajendran, “Detecting Dark Blobs,” *Phys. Rev. D* **98**, 115020 (2018), arXiv:1807.03788 [hep-ph].
- [13] Edward Hardy, Robert Lasenby, John March-Russell, and Stephen M. West, “Big Bang Synthesis of Nuclear Dark Matter,” *JHEP* **15**, 011 (2020), arXiv:1411.3739 [hep-ph].
- [14] Gordan Krnjaic and Kris Sigurdson, “Big Bang Dark-leosynthesis,” *Phys. Lett. B* **751**, 464–468 (2015), arXiv:1406.1171 [hep-ph].
- [15] George Gamow, *The Quantum Theory of the Atomic Nucleus* (US Atomic Energy Commission, Division of Technical Information Extension, 1963).
- [16] Cora Dvorkin, Kfir Blum, and Marc Kamionkowski, “Constraining Dark Matter-Baryon Scattering with Linear Cosmology,” *Phys. Rev. D* **89**, 023519 (2014), arXiv:1311.2937 [astro-ph.CO].
- [17] Yacine Ali-Haïmoud and Christopher M. Hirata, “Hyrec: A fast and highly accurate primordial hydrogen and helium recombination code,” *Phys. Rev. D* **83**, 043513 (2011), arXiv:1011.3758 [astro-ph.CO].
- [18] Nanoom Lee and Yacine Ali-Haïmoud, “Hyrec-2: A highly accurate sub-millisecond recombination code,” *Phys. Rev. D* **102**, 083517 (2020), arXiv:2007.14114 [astro-ph.CO].
- [19] Julian B. Muñoz and Abraham Loeb, “A small amount of mini-charged dark matter could cool the baryons in the early Universe,” *Nature* **557**, 684 (2018), arXiv:1802.10094 [astro-ph.CO].
- [20] Saurabh Singh *et al.*, “SARAS 2 constraints on global 21-cm signals from the Epoch of Reionization,” *Astrophys. J.* **858**, 54 (2018), arXiv:1711.11281 [astro-ph.CO].
- [21] DC Price, LJ Greenhill, Anastasia Fialkov, GIANNI Bernardi, H Garsden, BR Barsdell, J Kocz, MM Anderson, SA Bourke, J Craig, *et al.*, “Design and characterization of the large-aperture experiment to detect the dark age (leda) radiometer systems,” *Monthly Notices of the Royal Astronomical Society* **478**, 4193–4213 (2018).
- [22] Tabitha C. Voytek, Aravind Natarajan, José Miguel Jáuregui García, Jeffrey B. Peterson, and Omar López-Cruz, “Probing the Dark Ages at $z \sim 20$: The SCI-HI 21 cm All-sky Spectrum Experiment,” *Astrophys. J. Lett.* **782**, L9 (2014), arXiv:1311.0014 [astro-ph.CO].
- [23] Morgan E. Presley, Adrian Liu, and Aaron R. Parsons, “Measuring the Cosmological 21 cm Monopole with an Interferometer,” *Astrophys. J.* **809**, 18 (2015), arXiv:1501.01633 [astro-ph.CO].
- [24] Bang D. Nhan, Richard F. Bradley, and Jack O. Burns, “A polarimetric approach for constraining the dynamic foreground spectrum for cosmological global 21-cm measurements,” *Astrophys. J.* **836**, 90 (2017), arXiv:1611.06062 [astro-ph.IM].
- [25] Robert Lasenby, “Long range dark matter self-interactions and plasma instabilities,” *JCAP* **11**, 034 (2020), arXiv:2007.00667 [hep-ph].
- [26] Leonid Chuzhoy and Edward W. Kolb, “Reopening the window on charged dark matter,” *JCAP* **07**, 014 (2009), arXiv:0809.0436 [astro-ph].
- [27] David Dunskey, Lawrence J. Hall, and Keisuke Horigaya, “CHAMP Cosmic Rays,” *JCAP* **07**, 015 (2019), arXiv:1812.11116 [astro-ph.HE].
- [28] Roni Harnik, Ryan Plestid, Maxim Pospelov, and Harikrishnan Ramani, “Millicharged Cosmic Rays and Low Recoil Detectors,” (2020), arXiv:2010.11190 [hep-ph].
- [29] Timon Emken, Rouven Essig, Chris Kouvaris, and Mukul Sholapurkar, “Direct Detection of Strongly Interacting Sub-GeV Dark Matter via Electron Recoils,” *JCAP* **09**, 070 (2019), arXiv:1905.06348 [hep-ph].
- [30] Liron Barak *et al.* (SENSEI), “SENSEI: Direct-Detection Results on sub-GeV Dark Matter from a New Skipper-CCD,” *Phys. Rev. Lett.* **125**, 171802 (2020), arXiv:2004.11378 [astro-ph.CO].

- [31] A. Aguilar-Arevalo *et al.* (DAMIC), “Results on low-mass weakly interacting massive particles from a 11 kg-day target exposure of DAMIC at SNOLAB,” *Phys. Rev. Lett.* **125**, 241803 (2020), arXiv:2007.15622 [astro-ph.CO].
- [32] R. Agnese *et al.* (SuperCDMS), “Results from the Super Cryogenic Dark Matter Search Experiment at Soudan,” *Phys. Rev. Lett.* **120**, 061802 (2018), arXiv:1708.08869 [hep-ex].
- [33] Sinead Griffin, Simon Knapen, Tongyan Lin, and Kathryn M. Zurek, “Directional Detection of Light Dark Matter with Polar Materials,” *Phys. Rev. D* **98**, 115034 (2018), arXiv:1807.10291 [hep-ph].
- [34] Rouven Essig, Jesús Pérez-Ríos, Harikrishnan Ramani, and Oren Slone, “Direct Detection of Spin-(In)dependent Nuclear Scattering of Sub-GeV Dark Matter Using Molecular Excitations,” *Phys. Rev. Research.* **1**, 033105 (2019), arXiv:1907.07682 [hep-ph].
- [35] Philip C. Bunting, Giorgio Gratta, Tom Melia, and Surjeet Rajendran, “Magnetic Bubble Chambers and Sub-GeV Dark Matter Direct Detection,” *Phys. Rev. D* **95**, 095001 (2017), arXiv:1701.06566 [hep-ph].
- [36] Hao Chen, Rupak Mahapatra, Glenn Agnolet, Michael Nippe, Minjie Lu, Philip C. Bunting, Tom Melia, Surjeet Rajendran, Giorgio Gratta, and Jeffrey Long, “Quantum Detection using Magnetic Avalanches in Single-Molecule Magnets,” (2020), arXiv:2002.09409 [physics.ins-det].
- [37] Asher Berlin, Raffaele Tito D’Agnolo, Sebastian A. R. Ellis, Philip Schuster, and Natalia Toro, “Directly Deflecting Particle Dark Matter,” *Phys. Rev. Lett.* **124**, 011801 (2020), arXiv:1908.06982 [hep-ph].
- [38] Maxim Pospelov and Harikrishnan Ramani, “Earth-bound Milli-charge Relics,” (2020), arXiv:2012.03957 [hep-ph].